PAPER

Measurement of impurity lines with two-crystal x-ray spectrometers on EAST

View the article online for updates and enhancements.

Measurement of impurity lines with two-crystal x-ray spectrometers on EAST

Xinshuai YANG (杨新帅)[1], **Ruiji HU** (胡睿佶)[2], **Jun CHEN** (陈俊)[2],
Fudi WANG (王福地)[1], **Jia FU** (符佳)[1], **Yingying LI** (李颖颖)[1],
Hongming ZHANG (张洪明)[1], **Yongcai SHEN** (沈永才)[3],
Xianghui YIN (尹相辉)[4], **Bo LYU** (吕波)[1] **and EAST team**[1]

[1] Institute of Plasma Physics, Chinese Academy of Sciences, Hefei 230031, People's Republic of China
[2] Department of Engineering and Applied Physics, University of Science and Technology of China, Hefei 230026, People's Republic of China
[3] School of Physics and Electrical Engineering, Anqing Normal University, Anqing 246011, People's Republic of China
[4] School of Electrical Engineering, University of South China, Hengyang 421001, People's Republic of China

E-mail: blu@ipp.ac.cn

CrossMark

Abstract

To simultaneously measure the He-like and H-like argon spectra, a two-crystal assembly has been deployed to replace the previous single crystal on the tangential x-ray crystal spectrometer. By selecting appropriate crystals with similar Bragg angles, plasma temperature in the range of $0.5\,\mathrm{keV} \leqslant T_e \leqslant 10\,\mathrm{keV}$ and rotation can be diagnosed based on the He-like and H-like argon spectra. However, due to the added complexity in the two-crystal assembly in which the spectra might be diffracted by two crystals, some additional impurity lines were identified. For example, tungsten (W) lines in different ionization states were diffracted by the He-like and H-like crystal. Additional molybdenum (Mo) lines in the wavelength range of He-like and H-like argon spectra lines were also summarized. The existence of these additional lines caused the fitted temperature to be different from the true values. This paper presents the identified lines through a comparison with available database, which should be included in the fitting procedure.

Keywords: plasma diagnostics, x-ray two-crystal spectrometer, Doppler broadening, dielectronic satellite

(Some figures may appear in colour only in the online journal)

1. Introduction

X-ray crystal spectrometer (XCS) is one of the important methods for diagnosing and measuring tokamak plasma temperature and rotation velocities using Doppler broadening and frequency shift of characteristic spectral lines of certain impurity ions without adverse effects in plasma [1]. Currently, both tangential x-ray crystal spectrometer (TXCS) and poloidal x-ray crystal spectrometer (PXCS) were operational on EAST to measure plasma temperature and rotation velocities [2]. Based on the electron temperature range of tokamaks nowadays, crystal spectrometer normally measures He-like argon's dielectronic spectra [3]. Recently, the auxiliary heating

power such as electron cyclotron resonance heating (ECRH), ion cyclotron range of frequency (ICRF), lower hybrid current drive (LHCD) and neutral beam injection (NBI) had been significantly increased, and the plasma temperature has risen to several thousand electron volts on EAST. When electron temperature exceeds 3 keV, the relative concentration of He-like argon ions would become very small while the relative concentration of H-like argon ions increases [4], therefore, integrating both He-like and H-like argon crystals on a single spectrometer is necessary and feasible when choosing the proper combination of crystal types and Bragg angles [5]. The employment of two crystals with similar Bragg angles cannot only reduce the cost of constructing the crystal spectrometer,
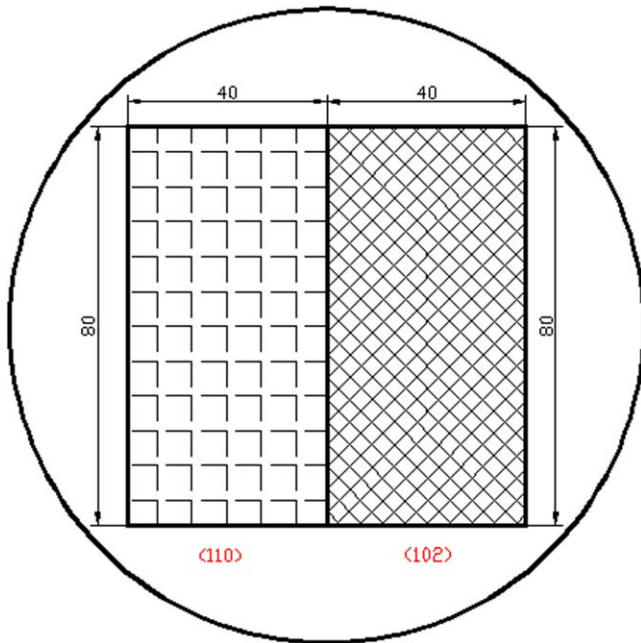
Figure 1. Simplified structure of double-crystal for TXCS. He-like crystal using quartz (110), $2d = 4.913$ Å, while H-like crystal using quartz (102), $2d = 4.562$ Å. The two spectral lines account for the width of the detector was 79 mm while the width of detector was 83.8 mm.

Figure 2. The original spectra of TXCS. He-like and H-like argon spectra are fully imaged on a pixel 487 (x) × 1891 (y) detector surface.

but also measure both high-quality He-like and H-like argon spectra simultaneously for plasma temperature up to 10 keV by exploiting the full width of a new large pixelated two-dimensional detector (PILATUS 900k, 83.8 × 325.3 mm^2). The two-crystal assembly has been commissioned on EAST and made successful measurement of He-like and H-like argon spectra that proved the feasibility of the two-crystal concept [6].

In the present experiments on EAST, most plasma-facing components were made of medium-Z and high-Z metals, possibly inducing metal impurities into plasmas. With two crystals, it also allowed more line emissions from other impurities such as Mo, Fe, W and Cu to be diffracted and mixed with the argon spectra at elevated temperature on EAST [6, 7]. This would also pose a challenge to the measurement of plasma temperature and rotation with two-crystal x-ray spectrometer due to polluted spectra from these unexpected lines. This paper reports the representative spectra containing impurity lines other than argon lines measured from the two-crystal spectrometer on EAST with identified impurity lines and their effect on temperature measurement.

2. Measurement of additional impurity lines on TXCS

The new two-crystal concept was first implemented on TXCS to deploy two crystals on a common glass substrate [8]. The selection of crystal type and geometric parameters were determined such that two spectra did not overlap on the detector and had the similar Bragg angle to fully exploit the limited width of the detector. A simplified schematic of
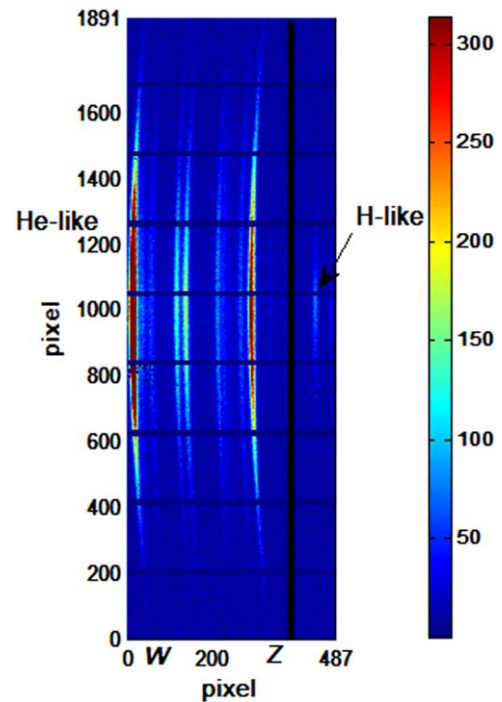
two-crystal setup for TXCS was shown in figure 1. From the chosen crystal parameters, it could be calculated that Bragg angle of two crystals are 53.5010° (110) and 54.3927° (102), respectively. These values were close enough to record two spectra that cover the detector width of ∼79 mm, which is within the width of detector (83.8 mm) [9, 10].

Figure 2 showed a time-integrated typical measurement of two argon spectra recorded for an L-mode discharge with $I_p \sim 450$ kA heated only with $P_{LHW} \sim 0.8$ MW using two-crystal x-ray spectrometers on EAST, where the color scale on the right represented the number of photons recorded. To the left of the black line is the He-like argon spectra diffracted from Quartz 110 crystals, and to the right of the black line is the H-like argon spectra diffracted from Quartz 102 crystal. It could be seen that the collected spectral lines were clearly separated and fully imaged on the detector. Figure 3 plotted the He-like and H-like argon spectra along the center chord averaged over the 100 pixel rows with typical line names labeled. It could be seen that for H-like argon spectra, the two Lyman-α (Lyα1 and Lyα2) lines' intensity was only vaguely visible in the center region of plasma and was much weaker than the resonance line (W), forbidden lines (Z), X and Y of He-like argon spectra due to relatively low electron temperature. However, as the heating power increased, the plasma temperature increased accordingly, and additional impurity lines in the spectra collected by the two-crystal x-ray spectrometer had been found [6].

Figure 4 showed two spectra with prominent impurity lines emitted from impurities other than argon. Due to the existence of these lines, ion temperature inferred from the He-like and H-like argon spectra was found to be in discrepancy,
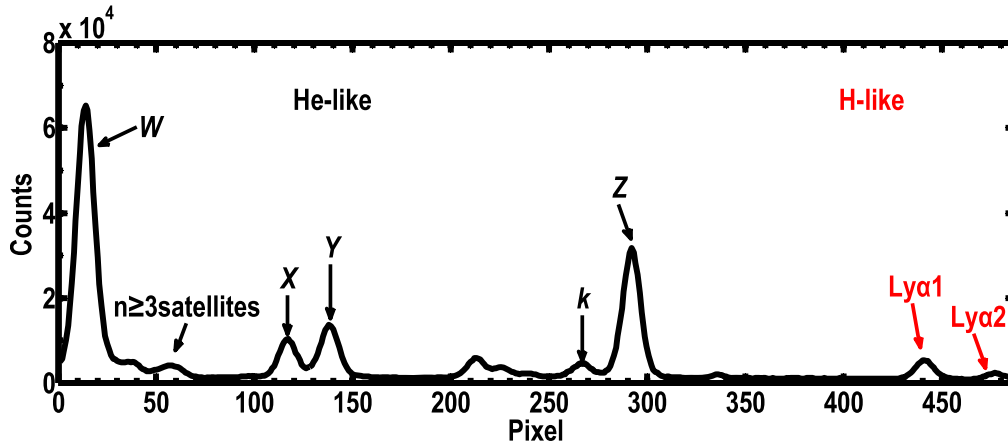
Figure 3. He-like and H-like argon spectra observed on the central sight line using two-crystal x-ray spectrometers on EAST. Because the plasma temperature was relatively low at present, the intensity of H-like argon spectrum line was not enough.
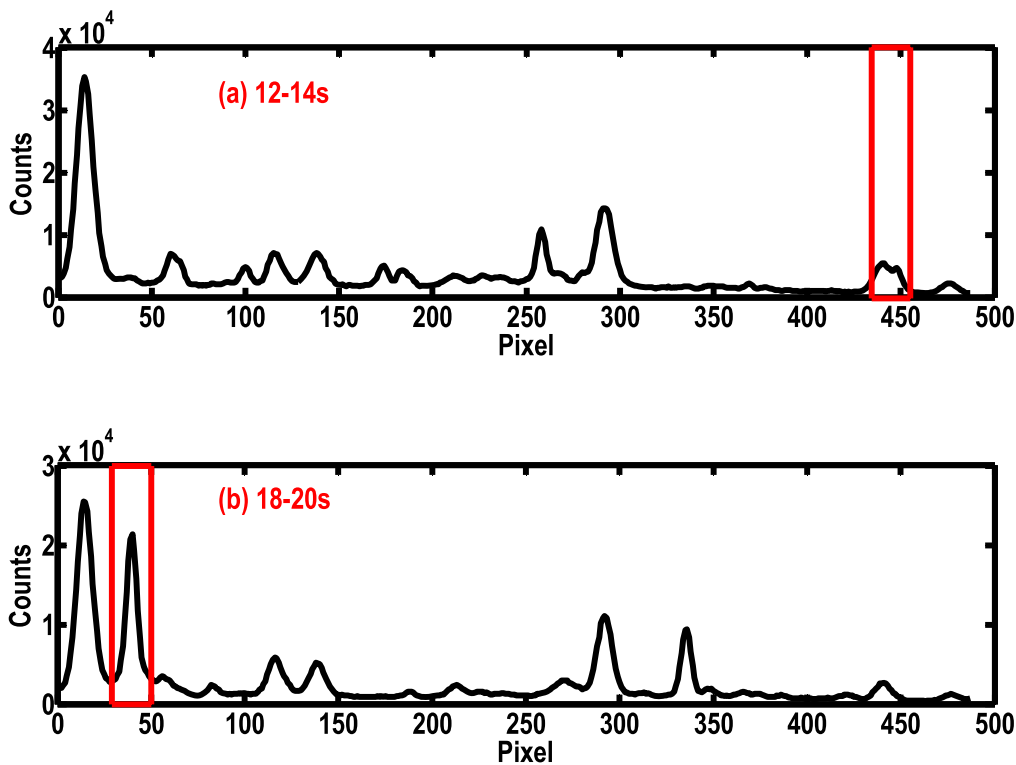

Figure 4. He-like and H-like argon spectra with other impurity lines. An impurity near Lyα1 line was shown in (a), an impurity near *W* line was shown in (b).

although for two-crystal x-ray spectrometers on EAST, argon ion temperature was expected to agree with each other for He-like and H-like argon ions [6]. For He-like and H-like argon spectra, ion temperature was normally derived from the Doppler broadening of *W* line and Lyman-α line, respectively.

Figure 5 plotted a discharge in which the inferred plasma temperatures were affected by these sporadic impurity lines. It could be seen that the ion temperature fitted by H-like argon spectra was obviously higher than that fitted by He-like argon spectra due to the existence of impurity line near Lyα1 line when the electron temperature was above 3 keV, since the additional line resulted in a bigger broadening. This indicated

that these lines needed to be identified and excluded from the spectral fitting.

3. Identification of impurity lines

Since the existence of impurity lines affected the fitting of spectra, to obtain the correct plasma temperature, identifying spectral lines and impurities were necessary for two-crystal x-ray spectrometer. This section presented the measured spectra from recent plasma operations with unforeseen lines that were present in the argon spectra and identification of these impurity lines.
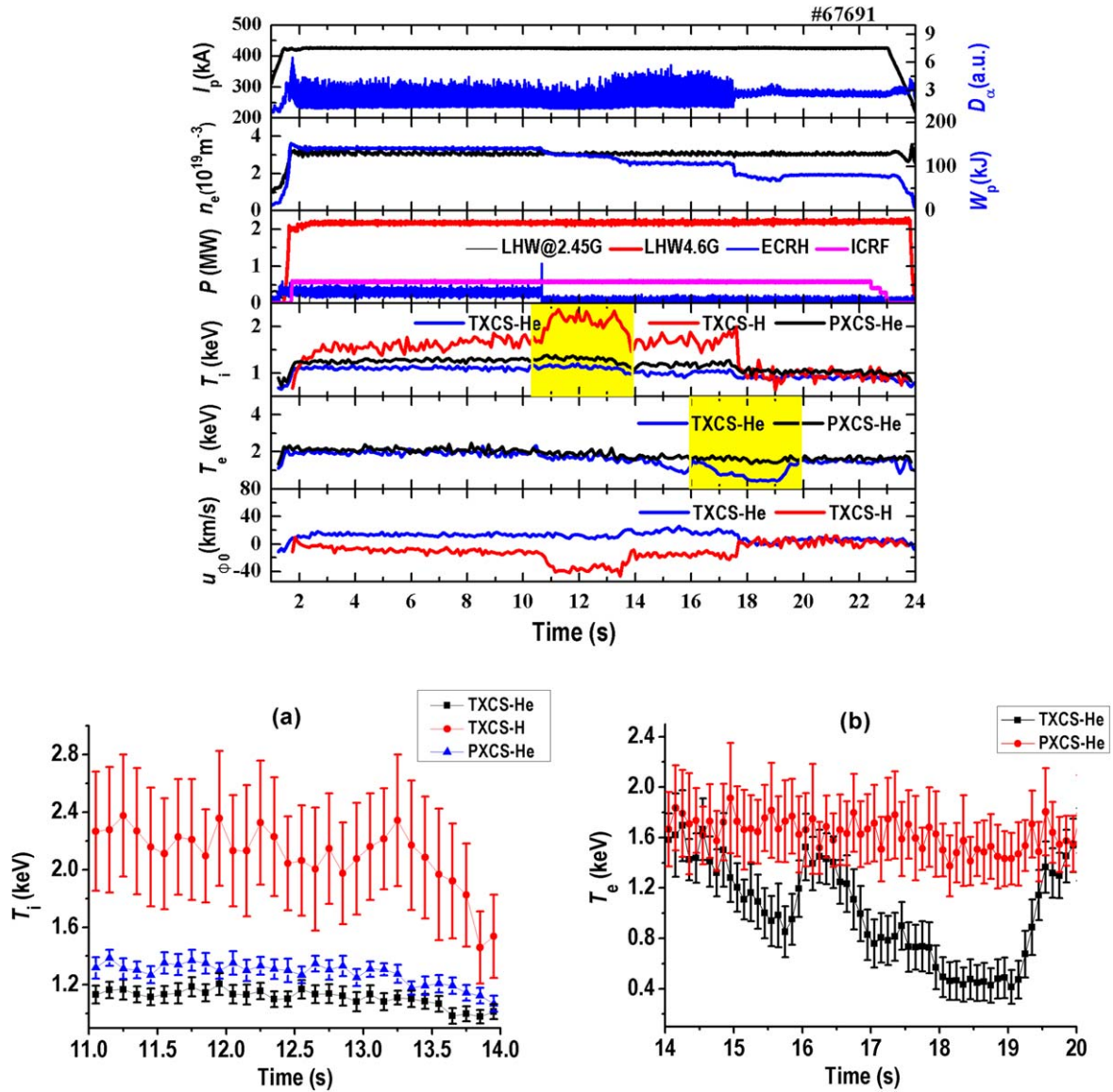
Figure 5. Information of the plasma parameters acquired from He-like and H-like argon spectra with impurity lines. Electron and ion temperature measurement using TXCS and PXCS with error bar. The ion temperature measured by three spectra from 11 to 14 s was shown in (a); electron temperature measured from 14 to 20 s was shown in (b).
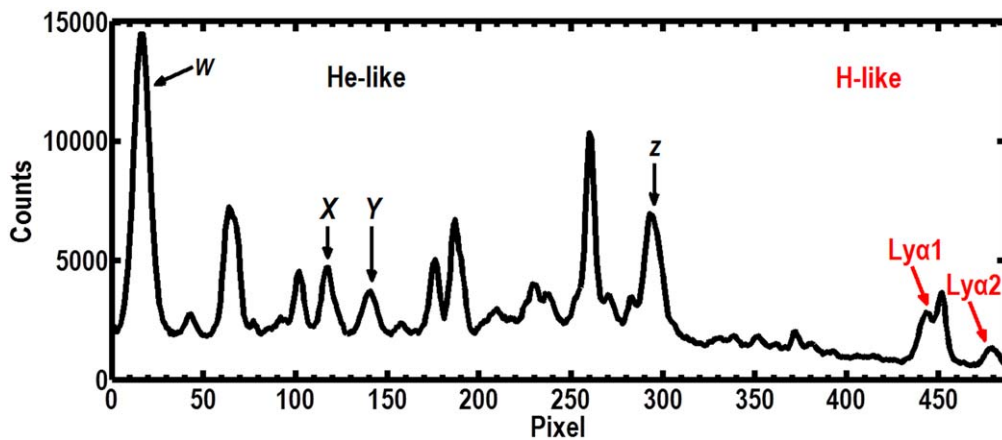

Figure 6. He-like and H-like argon spectra with other impurity lines.

(a) ion temperature profiles
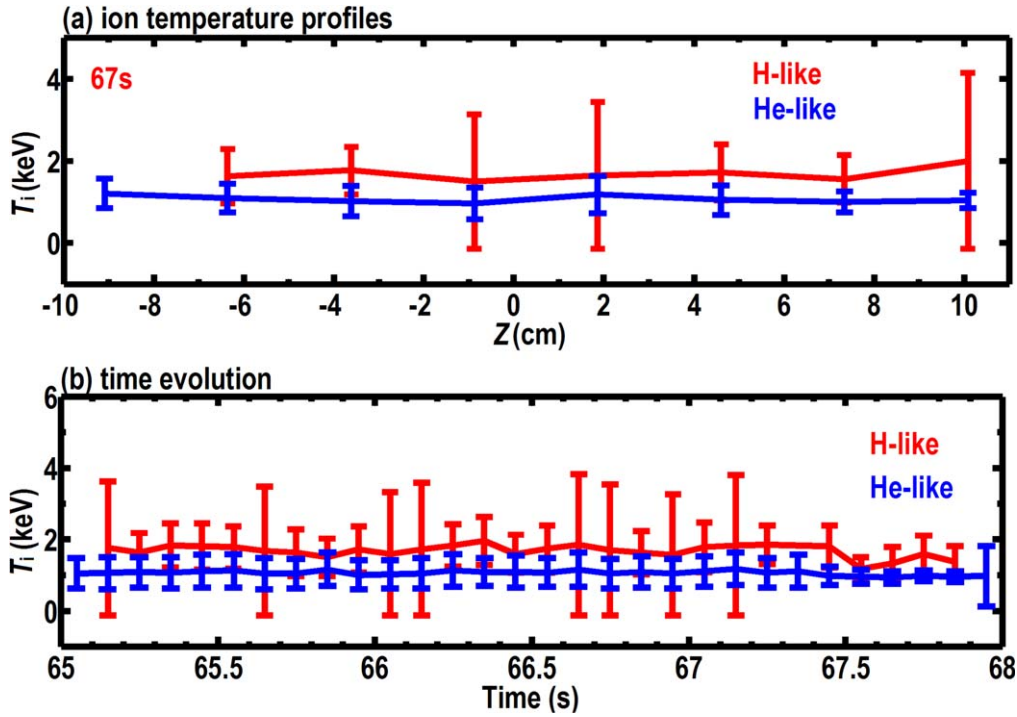

(b) time evolution

Figure 7. Ion temperature variation measured by H-like and He-like argon spectra. (a) Ion temperature profiles, (b) ion temperature evolution.

Figure 6 showed the spectra with visible impurity lines measured from $65\,\mathrm{s} \leqslant t \leqslant 68\,\mathrm{s}$ with 100 ms integration time each exposure for a long-pulse upper-single-null plasma on EAST (#73834) with $I_\mathrm{p} \sim 450\,\mathrm{kA}$, $n_\mathrm{e0} \sim 2.8 \times 10^{19}\,\mathrm{m}^{-3}$ heated by $P_\mathrm{LHW} \sim 1.7\,\mathrm{MW}$ and $P_\mathrm{ECRH} \sim 0.35\,\mathrm{MW}$. It could be seen that in the pixel space between those characteristic lines, several other prominent lines with different intensities were discovered, including one line on the short-wavelength side of the Lyα1 line and a peak located between the W line and $n \geqslant 3$ dielectronic satellites.

Figure 7 showed the ion temperature measured by these He-like and H-like argon spectra. The profile of ion temperature at 67 s was presented in (a) and the changes in the ion temperature measured at the plasma core from 65 to 68 s were presented in (b), where the $z = 0\,\mathrm{cm}$ is the mid-plane position, which corresponded to the center of the plasma. Here, the W line was simply fitted with the Voigt function taking into account its neighboring $n \geqslant 3$ satellites and an additional line between them, and the two Lyman-α lines were fitted together with Gaussian functions with a distinct line that is mixed with Lyα1 line. This way of fitting might mostly reduce the impact of impurity line on the ion temperature measurement. Ion temperature in the plasma core was close and the ion temperature in the range of $-6\,\mathrm{cm} < z < 10\,\mathrm{cm}$ was almost flat. It could be seen that the ion temperature measured from H-like argon spectra had bigger error bar and were larger than those obtained with He-like argon spectra in the plasma core. This was probably due to that the relative concentration of the He-like argon ions in the plasma core would evolve into a hollow profile when electron temperature was larger than 3 keV and the chord integral effect was obvious. On the other hand, the existence of the different
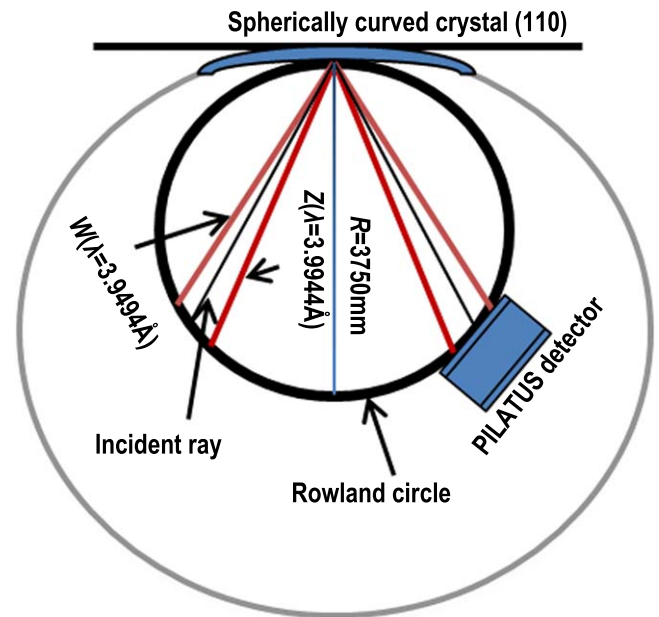

Figure 8. Simplified diagram of the diffraction structure of XCS. The wavelength scales were estimated based on the He-like and H-like argon spectra, utilizing the W line and Lyα1 line for reference to calculate each peak wavelength.

impurity lines affected the routine fitting of the spectral lines at different positions. At present, the spectra with visible impurity lines were measured without NBI injection and there is no any other diagnostics in ion temperature measurements can be compared. Comparative results have been discussed in another article [11] but the influence of impurity lines on temperature had not been excluded completely. To infer
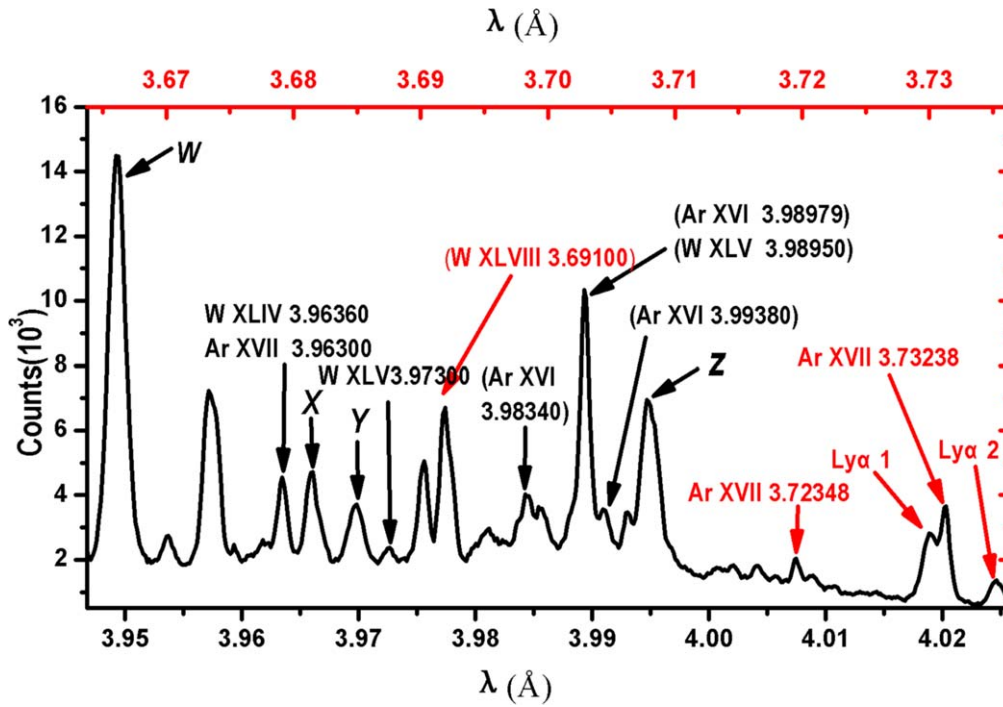
Figure 9. Spectrum for H-like and He-like argon spectra after identifying spectral lines and calibrating impurities. The bottom scale was based on He-like argon spectra and the top scale was based on H-like argon spectra. The impurity lines marked with red were diffracted by the H-like, while the lines marked with black were diffracted by the He-like. Such as the W XLVIII at 3.691 00 Å was diffracted by H-like crystal even though it was in the He-like argon spectrum.

correct ion temperature and electron temperature for the future EAST experiment, these impurity lines must be taken into account.

To assist the line identification, a simplified diagram of the diffraction geometry of XCS is shown in figure 8. It could be seen that the incident light from the center region of plasma struck on the spherical crystal and was captured by the detector through crystal diffraction, in which lines of different wavelengths would eventually be focused on different points in the Rowland circles. Because the wavelength of lines corresponds to the pixel location, taking the He-like argon spectra as an example and using the W and Z lines as the reference position, each peak wavelength can be calculated from the corresponding relationship between pixels and wavelength. According to the wavelength and the incident angle of the W line and Z line ($\lambda_w = 3.9494$ Å, $\lambda_z = 3.9944$ Å, $\theta_w = 53.5010°$, $\theta_z = 54.3927°$), the Bragg law and the focusing properties of spherical crystals, when assuming that the incident light pixel was P_λ, the incident angle θ_λ can be described by

$$\theta_\lambda = \theta_w + \Delta\theta = \theta_w + 180° \times (P_\lambda - P_w) \times \Delta x/(\pi \times R \sin\theta), \quad (1)$$

$$\lambda = 2d \sin\theta_\lambda, \quad (2)$$

where $\Delta x = 0.172$ mm was the distance between each pixel, $P_W = 17$ was W line pixel position, $2d = 4.913\,04$ Å, $\theta = (\theta_w + \theta_z)/2 = 53.946\,85°$ was the average Bragg angle of W line and Z line and $R = 3750$ mm was the radius of curvature of the spherical crystal. For the same principle,

the wavelength of the H-like argon spectra was measured according to the wavelength and the incident angle of the two Lyman-α line ($\lambda_{\text{Ly}\alpha1} = 3.730\,00$ Å, $\lambda_{\text{Ly}\alpha2} = 3.735\,30$ Å, $\theta_{\text{Ly}\alpha1} = 54.8432°$, $\theta_{\text{Ly}\alpha2} = 54.9589°$), where $2d = 4.562\,25$ Å. By comparing with the He-like argon spectra measured from the PXCS, it could be determined if the line was diffracted by He-like or H-like crystal.

The spectral lines measured by the two-crystal x-ray spectrometer were two independent diffraction systems, where each wavelength corresponding to the pixel was determined by its own Bragg angle. Since the lattice spacing of each crystal was different and the corresponding wavelengths of each pixel were different, two sets of coordinate systems can be set up for the same spectra line that the coordinate assignment of each peak can be calibrated and the wavelength of the peak can be determined simultaneously. Figure 9 plotted the spectra for He-like and H-like argon after identifying spectral lines and calibrating impurities and the wavelengths were matched with NIST Atomic Spectra Database to identify the possible lines. In the spectra, the top/red scale was based on H-like argon spectra while the bottom/black scale was based on He-like argon spectra, in which the impurities marked with black and red were obtained by the diffraction of He-like and H-like crystals, respectively.

4. Analysis of impurity lines

It could be seen from figure 9 that the impurity lines distributed in the whole spectra mainly represented tungsten (W)

Table 1. The possible types and wavelength ranges of impurities in the spectrum.

Helium-like (3.94675–4.02591 Å)			Hydrogen-like (3.66677–3.73647 Å)		
Ion	Observed wavelength (Å)	Ritz wavelength (Å)	Ion	Observed wavelength (Å)	Ritz wavelength (Å)
Ar XVII	3.94907	3.94907	W XLVI	3.60500	3.60500
Ar XVII	3.96300	3.96936	W XLVI	3.61890	3.61890
W XLIV	3.96360	3.96350	Mo XXXIII	3.63600	3.64000
Ar XVII		3.96586	Mo XLI		3.65427
Ar XVI		3.96760	W XLV	3.66200	3.66170
Ar XVI		3.96850	W LXIV		3.66500
Mo XL		3.97263	W XLVI	3.67500	3.66500
W XLV	3.97300	3.97300	Mo XXXIII	3.68400	3.68500
Ar XVI		3.98130	Mo XLII		3.68803
Ar XVI		3.98167	W XLVIII	3.69100	3.69100
Ar XVI		3.98340	Mo XLI		3.69596
Ar XVI		3.98572	Mo XLI		3.70656
W XLV	3.98950	3.98950	Mo XLI		3.70814
Ar XVI		3.98979	Mo XLI		3.70882
Ar XVI		3.98981	Mo XLI		3.70964
Ar XVI		3.99380	Ar XVII		3.72348
Ar XVI		3.99388	Ar XVIII	3.73110	3.73110
Ar XVII		3.99415	Ar XVII		3.73238
Ar XV	4.00000	4.00100	W LXIV		3.73600
Ar XV	4.00440	4.00360	Ar XVIII	3.73652	3.73652
Ar XVI		4.01038	W XLV	3.74000	3.73970
Ar XVI		4.01219	Ar XVII		3.74151
Ar XVI		4.01250			
Ar XV	4.01370	4.01370			
Ar XVI		4.01450			
Ar XVI		4.01480			
Ar XVI		4.01590			
Ar XVI		4.01631			
W XLIV	4.01700	4.01700			
W XLIII	4.01700	4.01700			
W XLIV	4.01700	4.01700			
Ar XV	4.02010	4.02010			
Ar XV	4.02720	4.02720			

and argon (Ar) [12] with different ionization stages. Here, the *W* line of He-like argon spectra had the maximum intensity at 3.949 40 Å, since the relative concentration of He-like argon ion was highest when the electron temperature was below 3 keV. A vaguely visible peak next was discovered but where this peak came from had not been confirmed previously. A preliminary search indicated that was mostly likely W XLVI at 3.675 00 Å diffracted by H-like crystal of the first order.

Additionally, the intensity of $n \geqslant 3$ satellites and *X* line was much higher than the previous experimental results. It was surmised that other impurity lines might overlap with them, which would have an effect on the fitting results of ion and electron temperature. The W XLIV at 3.963 60 Å and W XLV at 3.973 00 Å diffracted by He-like crystal of the first order were identified on the side of the *X* and *Y* lines, respectively, since the upper divertors on EAST contain a large amount of tungsten [13], and the existence of these tungsten lines were most likely due to the ionization of tungsten at high electron temperatures, especially during the H-mode phase. It is also noted that the W XLVIII at

3.691 00 Å marked in red indicated that this line was diffracted by H-like crystal though it was located in He-like argon spectra.

Furthermore, there was an impurity line on the side of *Z* line that was of the second highest intensity, which was initially identified as Ar XVI at 3.989 79 Å or W XLV at 3.989 50 Å diffracted by He-like crystal, and the intensity even exceeded that of the *Z* line. On the side of the Lyα1 line, Ar XVII at 3.732 38 Å diffracted by the H-like crystal at the first order was presented whose intensity was higher than the Lyα1 line. For x-ray crystal spectrometer, argon puffing was mainly used to measure the ion temperature and plasma rotation with argon spectra, so it is very likely that argon ions of different ionization states would be collected in the spectra at different temperatures.

Table 1 summarized the possible lines and wavelength ranges of impurities with He-like and H-like argon spectra. The wavelength range of He-like argon spectra is between 3.946 75 and 4.025 91 Å, and that of H-like argon spectra is between 3.666 77 and 3.736 47 Å, so other impurity lines in

this wavelength range are likely to be captured. It could be seen from the table that the impurities in this range are mainly W and Mo at different ionization stages. Because the current temperature is not high enough, some impurity lines are not labeled in He-like and H-like argon spectra. Also, some peaks with specific wavelengths in the spectra cannot be identified to the corresponding impurities at present, and requires further exploration. Additionally, because the vacuum chamber and LHCD, ICRF transmitting antenna use a large number of stainless steels with TiN coating, the secondary diffraction of Fe XXV at $1.850\,50$ Å might also occur in the plasma core and diffracted on the second-order [6].

5. Summary

Spectra with impurity lines measured from both He-like and H-like crystals using a two-crystal x-ray spectrometer on EAST were identified. The identification and calibration process of the spectral lines were also shown. Tungsten and argon as impurity ions with different ionization states were presented in the whole spectrum range, which affected the He-like and H-like argon spectra fitting to infer ion temperature but provided an opportunity to study impurity transportation in plasma in order to reduce the adverse effect of impurity on temperature measurement in the future EAST experiments.

References

[1] Bitter M *et al* 1979 *Phys. Rev. Lett.* **42** 304
[2] Wang F D 2012 The development of spherical curved crystal spectrometers and initial experimental results on spontaneous rotation on EAST *PhD Thesis* Institute of Plasma Physics, Chinese Academy of Sciences (in Chinese)
[3] Bitter M *et al* 1995 *Rev. Sci. Instrum.* **66** 530
[4] Marchuk O 2004 Modeling of He-like spectra measured at the TMarchuk, modeling of He-like spectra measured at the tokamak TEXTOR and TORE SUPRAEXTOR and SUPRA *PhD Thesis* Ruhr-Universität Bochum, Jülich
[5] Chen J *et al* 2015 *Nucl. Tech.* **38** 110403 (in Chinese)
[6] Lyu B *et al* 2016 *Rev. Sci. Instrum.* **87** 11E326
[7] Rice J E *et al* 2014 *J. Phys. B: At. Mol. Opt. Phys.* **47** 075701
[8] Lyu B *et al* 2014 *Rev. Sci. Instrum.* **85** 11E406
[9] Lyu B *et al* 2012 *Rev. Sci. Instrum.* **83** 10E130
[10] Shi Y J *et al* 2010 *Plasma Phys. Control. Fusion* **52** 085001
[11] Wang F D *et al* 2016 *Rev. Sci. Instrum.* **87** 11E342
[12] Rice J E *et al* 2011 *J. Phys. B: At. Mol. Opt. Phys.* **44** 165702
[13] Shen Y C *et al* 2015 *Plasma Sci. Technol.* **17** 183